Available online at www.sciencedirect.com

ScienceDirect

Journal of the European Ceramic Society 34 (2014) 925–931

www.elsevier.com/locate/jeurceramsoc

High temperature thermoelectric properties of $Ca_3Co_4O_{9+\delta}$ by auto-combustion synthesis and spark plasma sintering

NingYu Wu *, Tim C. Holgate, Ngo Van Nong, Nini Pryds, Søren Linderoth

Department of Energy Conversion and Storage, Technical University of Denmark, Frederiksborgvej 399, 4000 Roskilde, Denmark

Received 12 August 2013; received in revised form 10 October 2013; accepted 15 October 2013
Available online 9 November 2013

Abstract

A rapid method for the synthesis of $Ca_3Co_4O_{9+\delta}$ powder is introduced. The procedure is a modification of the conventional citric-nitrate sol–gel method where an auto-combustion process is initiated by a controlled thermal oxidation–reduction reaction. The resulting powders inherit the advantages of a wet chemical synthesis, such as morphological and compositional homogeneity, and fine, well-defined particle sizes coming from the controlled nature of the auto-combustion. Optimized spark plasma sintering (SPS) processing conditions were determined and used to fabricate dense and highly *c*-axis oriented samples. The microstructure and thermoelectric transport properties were determined both parallel (∥) and perpendicular (⊥) to the SPS pressure axis in order to investigate any possible anisotropy variations in the transport properties. At 800 °C, power factors of 506 μW/m K^2 (⊥) and 147 μW/m K^2 (∥), thermal conductivities values of 2.53 W/m K (⊥) and 1.25 W/m K (∥), and resulting figures-of-merit, *ZT*, of 0.21 (⊥) and 0.13 (∥) were observed.

Keywords: Thermoelectric; $Ca_3Co_4O_9$; Auto-combustion; Sol–gel; Citrate–nitrate; Spark plasma sintering

1. Introduction

Thermoelectric materials provide a mean to convert thermal energy into electrical energy via the Seebeck effect. The performance of a thermoelectric material can be evaluated by the dimensionless figure-of-merit $ZT = S^2T/\rho\kappa$, which consists of the Seebeck coefficient (S), electrical resistivity (ρ), thermal conductivity (κ) and absolute temperature (T). Oxides are one of candidates of high interest for thermoelectric applications due to their low cost, high-temperature stability in air and chemical inertness. Shikano et al. first brought attention to $Ca_3Co_4O_{9+\delta}$ as a high temperature thermoelectric p-type oxide candidate by reporting a ZT of 0.83 (at 800 °C) for a single crystalline sample.[1] $Ca_3Co_4O_{9+\delta}$ possesses a misfit-layered structure with a CdI_2-type hexagonal CoO_2 subsystem and a rock salt-type Ca_2CoO_3 subsystem that are alternately stacked along the *c*-axis with identical *a*, *c* and β parameters but different and incommensurate *b*1 and *b*2. Therefore, this misfit-layered oxide can be described with the formula $[Ca_2CoO_3]_{b1/b2}[CoO_2]$ with a *b*1 to *b*2 ratio of approximately 1.62.[2,3] The electronic conduction takes place mainly within the CoO_2 layer with the Ca_2CoO_3 layer serving as a charge reservoir, and while it is difficult to determine in which layer the lattice thermal conductivity is higher, the misfit between layers is expected to hinder the cross-plane phonon transport.[4] Therefore, anisotropy in the thermal and electrical transport properties is expected due to the two-dimensional character of this layered structure.[2,5–7]

At present, the fabrication of pure or doped $Ca_3Co_4O_{9+\delta}$ powders has mainly followed one of two routes: solid-state reaction or wet-chemical synthesis.[8–17] The advantages of the solid-state reaction are simplicity and high yield, but the purity and the homogeneity are two major issues of concern. By contrast, wet-chemical synthesis eliminates the drawbacks of the solid-state reaction by atomic scale mixing, but the low yield associated with this process limits the scalability. To retain the advantages of the wet-chemical synthesis, Song et al. reported the use of a polyacrylamide gel synthesis involving fast polymerization in calcium and cobalt nitrate aqueous solution, increasing the yield.[8] Zhang et al. also introduced a co-precipitation method to ensure the homogeneity of the powder.[9] Recently Wang et al. exhibited that via hydrothermal treatment the $Ca_3Co_4O_{9+\delta}$ particle size can be reduced further for better thermoelectric

* Corresponding author. Tel.: +45 46774942.
E-mail address: niwu@dtu.dk (N. Wu).

0955-2219/$ – see front matter © 2013 Elsevier Ltd. All rights reserved.
http://dx.doi.org/10.1016/j.jeurceramsoc.2013.10.022

properties.[16] Except for these unique methods, the Pechini method is still widely employed for $Ca_3Co_4O_{9+\delta}$ synthesis, which involves the chelation between citrate and the metal ions originating from dissolved metal nitrates.[18] Following the decomposition of the vaporization of the organic constituents and citrate complexes at elevated temperatures (400–500 °C), highly homogenous and sub-micron scale oxide powders can be obtained.[10] By this method, not only the atomic scale mixing for chemical homogeneity can be achieved, but also the feasibility of doping is provided by the introduction of dopant cation nitrates.[14] Despite the fact that this method is adaptable to many oxide systems, it still suffers from some practical difficulties, for instance, the resulting gel after drying is very adhesive and difficult to handle. Additionally, the gel swells considerably during the pyrolysis resulting in a drawn out and uneven reaction rather than a favoured rapid single step reaction. The present work sought to overcome these problems by using calcium and cobalt nitrates as the source of the metal ions, which were dissolved in a citric acid aqueous solution according to the Pechini method, but with a modified citrate-nitrate ratio that resulted in a rapid auto-combustion process induced by an exothermal oxidation-reduction reaction. The introduction of the auto-combustion step not only promotes the complete decomposition of the citrate complexes but also suppresses the grain growth by shortening the total reaction time at high temperature. The auto-combustion reaction was followed by the consolidation of the powders using spark plasma sintering (SPS) under different processing conditions. Due to the nature of the processing and the layered crystal structure of the material, the properties along both the parallel (∥) and perpendicular (⊥) directions relative to the SPS pressure axis were studied and are discussed in this paper.

2. Experimental procedure

A stoichiometric ratio of analytical regent grade $Ca(NO_3)_2{\cdot}4H_2O$ (99+ %) and $Co(NO_3)_2{\cdot}6H_2O$ (99+ %) was dissolved in an appropriate amount of distilled water, and a specific amount of citric acid (99+ %) was added to keep the citrate–metal cation molar ratio at 1:1. Additionally, the citrate-to-nitrate molar ratio was tuned by introducing different relative amounts of NH_4NO_3 (98+ %) ranging from 0.28 to 0.50. After initially drying the gel while stirring continuously at 75 °C until a uniform viscous gel was obtained, the hot plate temperature was raised to about 250 °C until the auto-combustion process was initiated, which was completed within a minute. The resulting powders were calcined at 750 °C for 2 h to obtain single phase $Ca_3Co_4O_{9+\delta}$.

Subsequently, the powders were consolidated by spark plasma sintering (SPS, Dr. Sinter SPS-515S, Fuji Electronic Industrial Co., Ltd.). Powders were poured into a graphite die to fabricate 10 mm thick pellets with a diameter of 18 mm. A pulsed electric current was then passed through the powders while under vacuum (10^{-3} bar) to consolidate the material. Based on our previous results, a range of the sintering temperatures were chosen from 700 to 850 °C, with a fixed uniaxial pressure of 50 MPa and a ramping rate of 100 °C/min. The sintering time was kept constant at 5 min.[16]

The SPS samples were cut in different directions as shown in Fig. 1 depending on the type of characterizations. The symbols "∥" and "⊥" are used to denote the properties measured along the directions parallel and perpendicular to the SPS pressure axis, respectively.

Simultaneous measurements of thermogravimetry (TG) and differential thermal analysis (DTA) were performed in oxygen with a heating rate of 10 °C/min on a Netzsch STA-449C. Additionally, the formation of the $Ca_3Co_4O_{9+\delta}$ phase from sol–gel produced precursors was analyzed by differential scanning calorimetry (DSC) using a Netzsch DSC-404C. After auto-igniting the sol–gel, the resulting powders were heated to 425 °C to remove any residual organics. A few milligrams of the product were lightly packed into an alumina-lined platinum crucible and loaded into the DSC. The measurement was performed under flowing air with a heating rate of 10 °C/min up to 825 °C.

X-ray diffraction (XRD) patterns were obtained using a Bruker D8 diffractometer with Cu Kα radiation. Microstructural analysis of the synthesized powders and the fracture surfaces of SPS samples was conducted using a ZEISS Supra 35 scanning electron microscope (SEM). The Seebeck coefficient (S) and electrical resistivity (ρ) measurements were carried out simultaneously with an ULVAC-RIKO ZEM3 from room temperature up to 800 °C under a low-pressure helium atmosphere.

The thermal conductivity was calculated using the equation $\kappa = \rho{\cdot}D{\cdot}c_v$ (where ρ, D *and* c_v are the density, thermal diffusivity and specific heat capacity, respectively). The thermal diffusivity was obtained under vacuum in a NETZSCH LFA-457 laser flash system. The c_v in this work was taken to be the temperature independent Dulong–Petit value of 0.798 J/g K. The bulk densities of the samples were measured by the Archimedes' method and compared with the theoretical density of $Ca_3Co_4O_9$, which is 4.68 g/cm^3 according to Masset et al.[2]

3. Result and discussion

According to Pederson' reaction model, the thermal oxidation-reduction reaction in a citrate-nitrate system can be represented by the following[19]:

$$9M(NO_3)_x + (5/2)xC_6H_8O_7 \rightarrow 15xCO_2 + (9/2)xN_2 + 10xH_2O + 9MO_{x/2}$$

where $\mathbf{M} = Ca^{2+}$ or Co^{2+}, $\boldsymbol{x} = 2$ for $Ca_3Co_4O_{9+\delta}$, and NO_3^- acts as the oxidant and citric acid as the fuel. The idealized combustion reaction occurs with a citrate-to-nitrate molar ratio of about 0.28. Through tuning this ratio, the auto-combustion flame propagation and the heat evolution can be controlled. In this work, a series of citrate-to-nitrate molar ratios were chosen from 0.50 to the ideal value 0.28. With a ratio of 0.50, no auto-combustion occurred. In contrast, the flame propagated rapidly and vigorously at the ideal ratio of 0.28. These observations are consistent with the conclusion reported by Roy et al. who studied the $YBa_2Cu_3O_{7-x}$ system[20]; the excessive amounts of

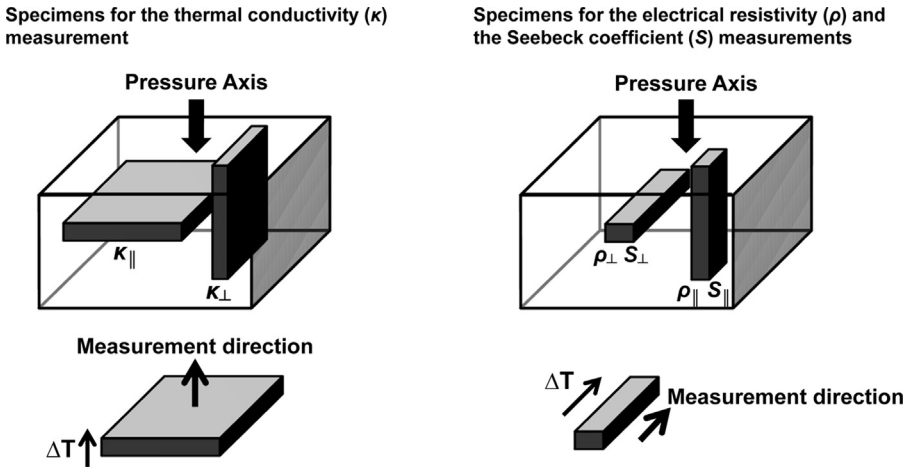

Fig. 1. Schematics of samples cut parallel (∥) and perpendicular (⊥) to the SPS pressure axis for the anisotropic thermoelectric properties measurements. The properties S, ρ and κ with subscript ∥ and ⊥ denote the properties measured along directions parallel and perpendicular to the SPS pressure axis.

citric acid cannot induce the auto-combustion and the maximum heat evolution happens when the citric acid amount is slightly higher than the stoichiometric nitrate requirement. To promote complete chelation, the $Ca_3Co_4O_{9+\delta}$ powders were synthesized from gels with an excess amount of citric acid so that the citrate-to-metal cation molar ratio was 1, and the necessary amount of nitrate required to activate the auto-combustion was provided by NH_4NO_3 to give a citrate-to-nitrate molar ratio of 0.40.

Fig. 2(a) shows the TG/DTA curve of a dry $Ca_3Co_4O_{9+\delta}$ gel with a citrate-to-nitrate molar ratio of 0.40. The DTA curve can be divided into three main regions. Below 200 °C there are three peaks, one endothermic at 100 °C and two exothermic, at 150 and 190 °C, accompanied by about 75% weight loss. These peaks can be ascribed to the evaporation of residual water, the partial decomposition of nitrate and the initiation of the auto-combustion reaction, respectively.[20] In the second region from 250 to 350 °C one broad exothermic peak can be observed, which may be attributed to the decomposition of residual citric acid and results in an additional ~2% weight loss. No exothermic peaks were observed between 400 and 500 °C indicating no residual citrate complexes. With the incorporation of the auto-combustion reaction, the starting precursors – $CaCO_3$ and Co_3O_4 – can be obtained at relatively low temperatures. The endothermic peak in the DSC curve displayed in Fig. 2(b) is a composite peak originating from the breakdown of $CaCO_3$ into CaO followed by the formation of the $Ca_3Co_4O_{9+\delta}$ phase. Although not presented here, comparison of the XRD patterns of the precursors after the initial furnace treatment at 425 °C with those of the sample reacted in the DSC confirm the origin of the peak to be a result of the formation of $Ca_3Co_4O_{9+\delta}$.

XRD patterns of the $Ca_3Co_4O_{9+\delta}$ powders as-synthesized and after SPS consolidation at 850 °C are shown in Fig. 3. All the

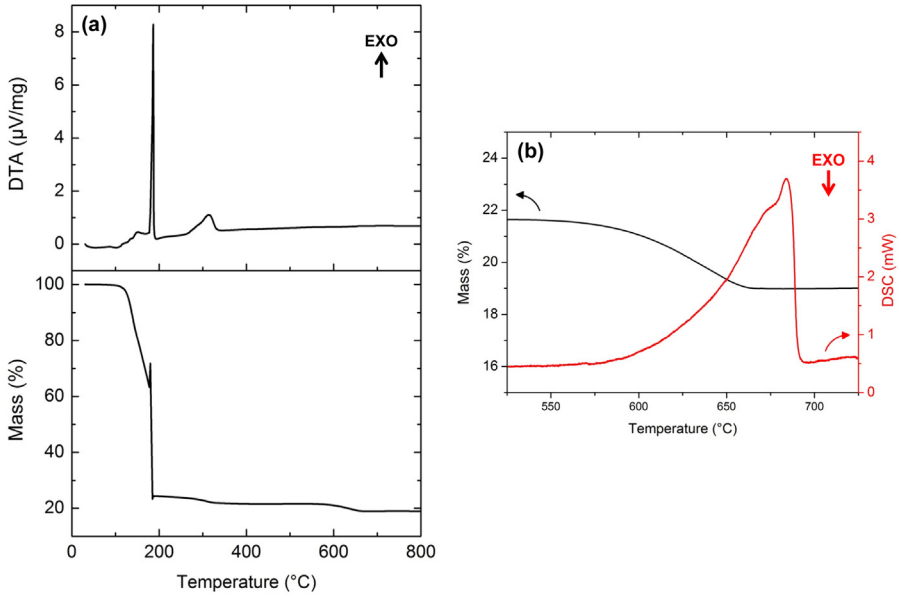

Fig. 2. (a) TG/DTA curves of the dry $Ca_3Co_4O_{9+\delta}$ citric-nitrate gel, and (b) the enlarged region of the TGA curve from (a) overlaid with the independently DSC measurement exhibiting a complex peak originating from the thermal decomposition of $CaCO_3$ to CaO and the formation of the $Ca_3Co_4O_{9+\delta}$ phase.

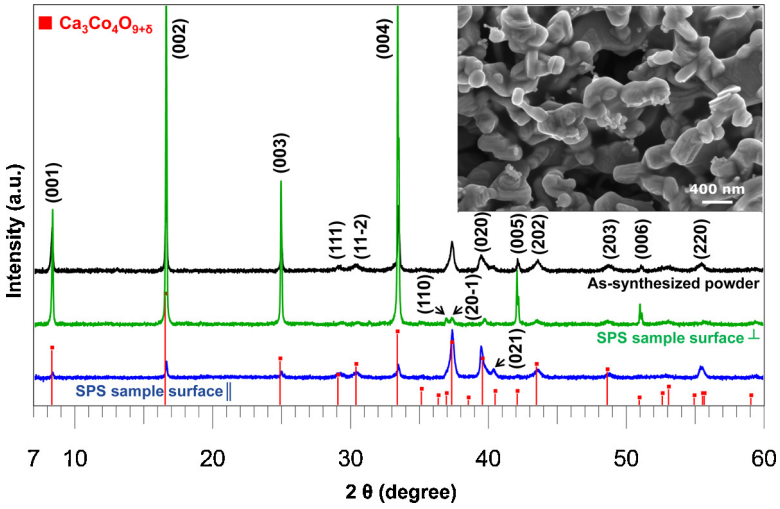

Fig. 3. XRD patterns of the as-synthesized $Ca_3Co_4O_{9+\delta}$ powders and the SPS consolidated samples. The red line pattern is from JCPDS PDF # 21-0139 for $Ca_3Co_4O_{9+\delta}$ phase identification. The inset is the SEM micrograph of the as-synthesized powders. (For interpretation of the references to colour in this figure legend, the reader is referred to the web version of this article.)

peaks could be indexed as $Ca_3Co_4O_9$ according to the JCPDS PDF # 21–0139 of $Ca_9Co_{12}O_{28}$ and the XRD patterns reported in the literature, indicating the purity and obvious texturing of these samples.[2] The inset in Fig. 3 displays the SEM micrographs of as-synthesized $Ca_3Co_4O_{9+\delta}$ particles with the average particle size of ~300 to 400 nm and a plate-like morphology. Fig. 4 shows a set of SEM micrographs of the sintered fracture surfaces after SPS processing at 850 °C for 5 min, which were observed along directions parallel and perpendicular to the SPS pressure axis. The platelet morphology and textured microstructure is observable in these two micrographs, which is also consistent with the anisotropic XRD results. All samples exhibited densities more than 99% of the theoretical density, and these values agree with Liu et al., Kenfaui et al. and our previous works.[16,21,22]

Due to the layered structure of $Ca_3Co_4O_{9+\delta}$ and the morphological anisotropy observed in this study, the thermoelectric properties were measured along both ⊥ and ∥ directions. Among samples which were densified by SPS at 700, 750, 800 and 850 °C, the maximum deviation from the averages in the ⊥ direction electrical resistivity, the Seebeck coefficient and the thermal conductivity are 2.5%, 1.1% and 2.2%, respectively, as measured at 700 °C (detailed data can be found in the appendix). These are all within the error of the measurements, and so to be consistent with our previous work on optimizing the SPS processing conditions for solid-state prepared $Ca_3Co_4O_{9+\delta}$. For simplicity, Fig. 5 shows only the results of the measurements performed on the sample processed by SPS at 850 °C for 5 minutes under 50 MPa of pressure.[16] The electrical resistivity in the plane perpendicular to the SPS pressure axis ($\rho\perp$) varied between 5.24 mΩ cm and 5.72 mΩ cm throughout the measured temperature regime with a minimum value of 5.24 mΩ cm at 650 °C. These results are lower than those observed by Zhang et al. on a sample synthesized by the conventional citrate-nitrate method – 6.13 mΩ cm at 700 °C.[6] To our knowledge, so far this is the lowest electrical resistivity value for pure polycrystalline $Ca_3Co_4O_{9+\delta}$ with the normal SPS processing. The electrical resistivity measured along the ∥ direction ($\rho\parallel$) was found to be 15.32 mΩ cm at 700 °C, which is below the previous reported value of about 18 mΩ cm at that temperature.[6] The low magnitude and high anisotropy of the electrical resistivity can be explained as a result of the enhanced morphological texturing of the sample. A quantitative analysis of the texturing can be obtained by assessing the volume fraction, $\boldsymbol{\alpha}_{(00l)}$, of *c*-axis oriented grains in the samples after SPS processing using the following equation[23]:

$$\alpha_{(00l)} = \frac{\sum(\boldsymbol{I}_{00l}/\boldsymbol{I}^*_{00l})}{\sum(\boldsymbol{I}_{hkl}/\boldsymbol{I}^*_{hkl})}$$

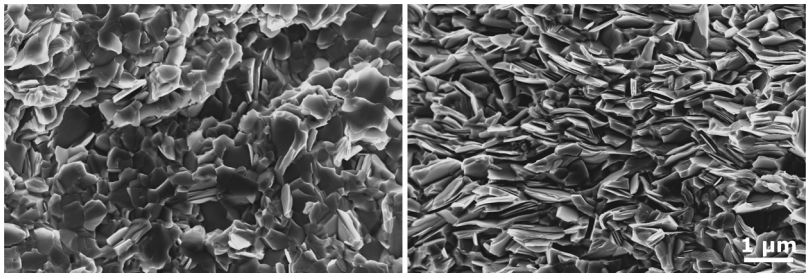

Fig. 4. SPS sample microstructure micrographs observed along directions parallel (left) and perpendicular (right) to the SPS pressure axis.

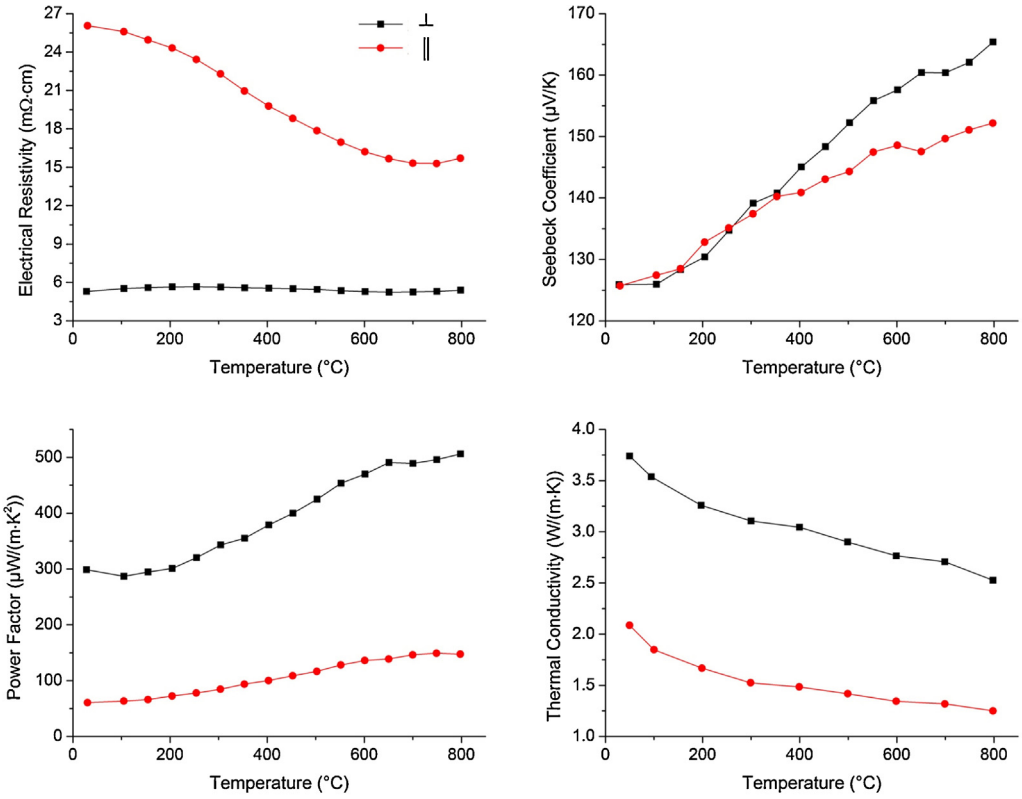

Fig. 5. The temperature dependence of the thermoelectric properties measured along the ⊥ and ∥ directions.

where $\boldsymbol{I}_{hkl}$ stands for the measured intensity of the (*hkl*) peaks from the XRD spectrum of the surface perpendicular to the SPS pressure axis of the consolidated samples and $\boldsymbol{I}^{*}_{hkl}$ for those of the as-synthesized $Ca_3Co_4O_{9+\delta}$ powders. The auto-combustion powders exhibit a significant $\alpha_{(00l)}$ value of up to 91%, which is consistent with high degree of texturing indicated by the SEM observations. Due to the plate-like morphology of the as-synthesized $Ca_3Co_4O_{9+\delta}$ powders shown in the inset of Fig. 3, asymmetric necking during sintering occurs resulting in anisotropic surface energies that in turn produce torques to drive the grain rotation.[24] Therefore, sintering with small plate-like $Ca_3Co_4O_{9+\delta}$ particles may enhance microstructural anisotropy as the higher density of grain boundaries results in a higher concentration of grain rotation driving forces and therefore a higher degree of grain alignment. A benefit of the auto-combustion reaction is the rapid formation of the starting precursors at relatively low temperatures. This allows for the subsequent calcination period needed to achieve the $Ca_3Co_4O_{9+\delta}$ phase formation to be kept relatively short (2 h in this work). This limits the high temperature (above 700 °C) particle size growth and therefore results in the enhancement of the anisotropy of the microstructure and the thermoelectric properties of the consolidated bulk samples. This conclusion corresponds well to Chen et al. work on the relationship between varied $Ca_3Co_4O_{9+\delta}$ calcination temperatures and particle sizes, which points out that the smallest $Ca_3Co_4O_{9+\delta}$ particle size calcinated at lower temperature after sintering exhibited the better grain alignment and higher thermoelectric performance.[25] The similar electrical conductivity improvement resulted from enhancing texturing also can be observed from other works. Both of Liu et al. and Kenfaui et al. works agreed that the SPS densification could improve the thermoelectric properties with grain orientation and higher bulk density.[21,26] With the assistance of the magnetic alignment technique and SPS processing, Zhou et al. reported a ρ⊥ of about 6 mΩ cm at 700 °C – exhibiting an improvement of about 30% compared with the less textured sample.[27] Lin et al. later proposed that fabricating $Ca_3Co_4O_{9+\delta}$ by the SPS and a dynamic forging process can increase grain orientation, also increasing the electrical conductivity by about 30%.[28] Recently, Noudem et al. enhanced the texturing by a modified SPS processing – so-called "edge free" spark plasma sintering, and at 550 °C a 30% improvement in the electrical resistivity (7 mΩ cm) and a power factor of 400 μW/m K^2 was be obtained.[29] Except SPS processing, the reactive-templated grain growth (RTGG) method is a means to achieve highly texturing $Ca_3Co_4O_{9+\delta}$ and it also demonstrated that the lowest electrical resistivity was from the most textures sample, yielding a resistance of 3.8 mΩ cm at about 800 °C.[30–33]

The temperature dependence of the Seebeck coefficient and power factor ($PF = S^2/\rho$) along both directions can also be seen in Fig. 5. The Seebeck coefficient increases with temperature, and the anisotropy between ⊥ and ∥ directions is not as pronounced as much as the electrical resistivity, which is consistent with the results of Tani et al. and Zhang et al. reporting the Seebeck coefficient to be insensitive to the grain orientation.[6,30] The highest Seebeck coefficient value of 165 μV/K was measured at 800 °C within the ⊥ direction, which is comparable with reported values of samples synthesized by wet-chemical methods.[6,8,9] Due

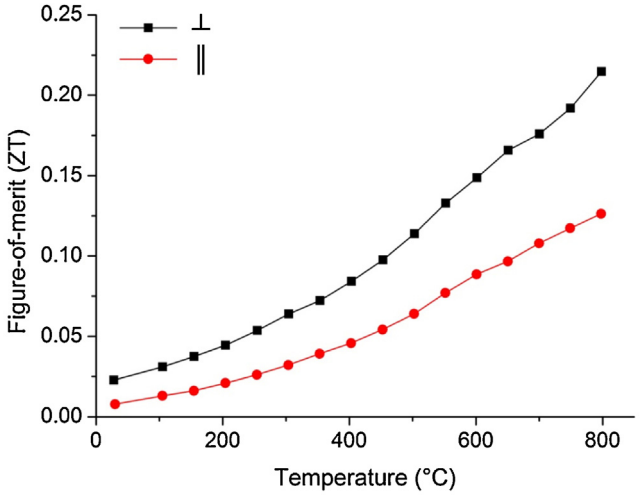

Fig. 6. The temperature dependence of the ZT measured along the ⊥ and ∥ directions.

to the lower ρ and higher S within the ⊥ plane, $PF\perp$ remains higher than $PF\parallel$ throughout the whole temperature range with a maximum value of $PF\perp \approx 500\ \mu W/m\ K^2$ at 800 °C. At 700 °C the value is ~490 $\mu W/m\ K^2$ – about 10% higher than reported for samples produced by the conventional citrate-nitrate reaction (about 445 $\mu W/m\ K^2$) with similar SPS condition.[6] This enhanced $PF\perp$, which was obtained by the auto-combustion synthesis and normal SPS processing, approaches that of samples prepared by more time costly processes such as the RTGG processing and repeated hot-pressing.[7,30,31,33]

The thermal conductivities (κ) measured along ⊥ and ∥ directions shown also in Fig. 5 decrease with the temperature, which is comparable with the reported results from $Ca_3Co_4O_{9+\delta}$ single crystal and polycrystalline samples.[1,7] κ contains both the electronic (κ_e) and the lattice (κ_L) contributions (i.e., $\kappa = \kappa_e + \kappa_L$), but by applying the Wiedemann–Franz relationship, $\kappa_e = L_0\, T/\rho$, where the Lorenz factor is taken as $L_0 = 2.45 \times 10^{-8}\ V^2/K^2$, the lattice contribution was calculated and accounts for more than 80% of the total in both directions.[1,4,34] Since $Ca_3Co_4O_{9+\delta}$ consists of alternating misfit-layers of CoO_2 and Ca_2CoO_3, anisotropy in the thermal and electrical transport properties is expected. Although achieving lower $\rho\perp$ by enhancing grain alignment is a promising and effective route to obtaining higher $PF\perp$, it will lead to the increase of the κ_e contribution in total κ and compromise the thermoelectric performance in $ZT\perp$, which may be observed from works with the RTGG processing and repeated hot-pressing.[7,31] The relationship of the degree of texturing and the anisotropy in the transport properties will be the focus of future studies.

Fig. 6 displays the temperature dependence of ZT calculated for both directions. At 800 °C, $ZT\perp$ and $ZT\parallel$ were found to be 0.21 and 0.13, respectively, and these values are among the highest ZT values reported for pure bulk polycrystalline $Ca_3Co_4O_{9+\delta}$ – comparable to those synthesized via the hydrothermal treatment ($ZT\perp \approx 0.27$ at 750 °C,Ref. 16), or processed with the RTGG ($ZT\perp \approx 0.26$ at 800 °C,Refs. 30,33) and repeated hot-pressing ($ZT\perp \approx 0.24$ at 800 °C,Ref. 7). However, it should be noted that the in-plane thermal conductivity used for the calculation of $ZT\perp$ of the sample produced by RTGG was measured on a sample exhibiting a lower electrical conductivity (and therefore a lower electronic contribution to the thermal conductivity) than the sample from which the power factor was taken.[31] Also, the value of $ZT\perp$ at 800 °C of the sample prepared by repeated hot-pressing was extrapolated from a fit equation provided in the reference – the measured data only extends to 650 °C.[7] When considering that the ratio of $ZT\perp/ZT\parallel$ and $PF\perp/PF\parallel$ are 1.62 and 3.44, the ⊥ plane can be expected to be a preferred direction for preparing thermoelectric legs.

4. Conclusion

In this work, a new rapid synthesis method of producing $Ca_3Co_4O_{9+\delta}$ fine powders using an auto-combustion synthesis method is demonstrated. The auto-combustion is induced by carefully tuning the ratio of citrate to nitrate based on the conventional sol–gel process. The synthesized $Ca_3Co_4O_{9+\delta}$ powders were consolidated by SPS and the anisotropic thermoelectric properties were measured parallel and perpendicular to the SPS pressure axis. The auto-combustion synthesis provides an efficient and rapid method for producing pure polycrystalline $Ca_3Co_4O_{9+\delta}$ with a high power factor and ZT in the plane perpendicular to the SPS pressure axis of about 500 $\mu W/m\ K^2$ and 0.21 at 800 °C, respectively. Moreover, the auto-combustion synthesis can be applied not only to pure but also doped $Ca_3Co_4O_{9+\delta}$ for further thermoelectric performance improvement.

Acknowledgement

The authors would like to thank Xiao Tang for the TG/DTA measurements and the Programme Commission on Energy and Environment (EnMi), which is part of the Danish Council for Strategic Research (Contract No. 10-093971) for sponsoring the OTE-POWER research work.

Appendix A. Supplementary data

Supplementary material related to this article can be found, in the online version, at http://dx.doi.org/10.1016/j.jeurceramsoc.2013.10.022.

References

1. Shikano M, Funahashi R. Electrical and thermal properties of single-crystalline $(Ca_2CoO_3)_{0.7}CoO_2$ with a $Ca_3Co_4O_9$ structure. *Appl Phys Lett* 2003;**82**:1851–3.
2. Masset AC, Michel C, Maignan A, Hervieu M, Toulemende O, Studer F, et al. Misfit-layered cobaltite with an anisotropic giant magnetoresistance: $Ca_3Co_4O_9$. *Phys Rev B* 2000;**62**:166–75.
3. Miyazaki Y, Onoda M, Oku T, Kikuchi M, Ishii Y, Ono Y, et al. Modulated structure of the thermoelectric compound $[Ca_2CoO_3]_{0.62}CoO_2$. *J Phys Soc Jpn* 2002;**71**:491–7.
4. Miyazaki Y, Kudo K, Akoshima M, Ono Y, Koike Y, Kajitani T. Low-temperature thermoelectric properties of the composite crystal $[Ca_2CoO_{3.34}]_{0.614}[CoO_2]$. *Jpn J Appl Phys* 2000;**39**:L531–3.
5. Bhattacharya S, Aswal DK, Singh A, Thinaharan C, Kulkarni N, Gupta SK, et al. Anisotropic electrical transport studies of $Ca_3Co_4O_9$ single crystals grown by the flux method. *Cryst Growth* 2005;**277**:246–51.

6. Zhang Y, Zhang J, Lu Q. Synthesis of highly textured $Ca_3Co_4O_9$ ceramics by spark plasma sintering. *Ceram Int* 2007;**33**:1305–8.
7. Kenfaui D, Lenoir B, Chateigner D, Ouladdiaf B, Gomina M, Noudem JG. Development of multilayer textured $Ca_3Co_4O_9$ materials for thermoelectric generators: Influence of the anisotropy on the transport properties. *J Eur Ceram Soc* 2012;**32**:2405–14.
8. Song Y, Nan CW. Preparation of $Ca_3Co_4O_9$ by polyacrylamide gel processing and its thermoelectric properties. *J Sol–Gel Sci Technol* 2007;**44**:139–44.
9. Zhang Y, Zhang J. Rapid reactive synthesis and sintering of textured $Ca_3Co_4O_9$ ceramics by spark plasma sintering. *J Mater Process Technol* 2008;**208**:70–4.
10. Zhang YF, Zhang JX, Lu QM, Zhang QY. Synthesis and characterization of $Ca_3Co_4O_9$ nanoparticles by citrate sol–gel method. *Mater Lett* 2006;**60**:2443–6.
11. Nong NV, Yanakiya S, Monica S, Pryds N, Ohtaki M. High-temperature thermoelectric and microstructural characteristics of cobalt-based oxides with Ga substituted on the Co-site. *J Electron Mater* 2011;**40**:716–22.
12. Nong NV, Liu C, Ohtaki M. High-temperature thermoelectric properties of late rare earth-doped $Ca_3Co_4O_{9+\delta}$. *J Alloys Compd* 2011;**509**:977–81.
13. Nong NV, Pryds N, Linderoth S, Ohtaki M. Enhancement of the thermoelectric performance of *p*-type layered oxide $Ca_3Co_4O_{9+\delta}$ through heavy doping and metallic nanoinclusions. *Adv Mater* 2011;**23**:2484–90.
14. Ou Y, Peng J, Li F, Yu ZX, Ma FY, Xie SH, et al. The effects of dual doping on the thermoelectric properties of $Ca_{3-x}M_xCo_{4-y}Cu_yO_9$ (M = Na La). *J Alloys Compd* 2012;**526**:139–44.
15. Sotelo A, Constantinescu G, Rasekh S, Torres MA, Diez JC, Madrea MA. Improvement of thermoelectric properties of $Ca_3Co_4O_9$ using soft chemistry synthetic methods. *J Eur Ceram Soc* 2012;**32**:2415–22.
16. Wang Y, Sui Y, Li F, Xu L, Wang X, Su W, et al. Thermoelectrics in misfit-layered oxides $[(Ca\,Ln)_2CoO_3]_{0.62}[CoO_2]$: from bulk to nano. *Nano Energy* 2012;**1**:456–65.
17. Wu NY, Holgate TC, Nong NV, Pryds N, Linderoth S. Effects of synthesis and spark plasma sintering conditions on the thermoelectric properties of $Ca_3Co_4O_{9+\delta}$. *J Electron Mater* 2013;**42**:2134–42.
18. Pechini MP. Method of Preparing Lead and Alkaline Earth Titanates and Niobates and Coating Method Using the Same to Form a Capacitor. United States patent US 003330697. 1967 July 11.
19. Pederson LR, Maupin GD, Weber WJ, McReady DJ, Stephens RW. Combustion synthesis of $YBa_2Cu_3O_{7-x}$: glycine/metal nitrate method. *Mater Lett* 1991;**10**:437–43.
20. Roy S, Sharma AD, Roy SN, Maiti HS. Synthesis of $YBa_2Cu_3O_{7-x}$ powder by autoignition of citrate–nitrate gel. *J Mater Res* 1993;**8**:2761–6.
21. Liu Y, Lin Y, Shi Z, Nan CW. Preparation of $Ca_3Co_4O_9$ and improvement of its thermoelectric properties by spark plasma sintering. *J Am Ceram Soc* 2005;**88**:1337–40.
22. Kenfaui D, Bonnefont G, Chateigner D, Fantozzi G, Gomina M, Noudem JG. $Ca_3Co_4O_9$ ceramics consolidated by SPS process: optimisation of mechanical and thermoelectric properties. *Mater Res Bull* 2010;**45**:1240–9.
23. Lotgering FK. Topotactical reactions with ferrimagnetic oxides having hexagonal crystal structures-I. *J Inorg Nucl Chem* 1959;**9**:113–23.
24. Wakai F, Fukutome H, Kobayashi N, Misaki T, Shinoda Y, Akatsu T, et al. Direct observation of sintering mechanics of a single grain boundary. *Acta Mater* 2012;**60**:507–16.
25. Chen S, Song X, Chen X, Chen Y, Barbero EJ, Thomas EL, et al. Effect of precursor calcination temperature on the microstructure and thermoelectric properties of $Ca_3Co_4O_9$ ceramics. *J Sol–Gel Sci Technol* 2012;**64**:627–36.
26. Kenfaui D, Chateigner D, Gomina M, Noudem JG. Texture, mechanical and thermoelectric properties of $Ca_3Co_4O_9$ ceramics. *J Alloys Compd* 2010;**490**:472–9.
27. Zhou Y, Matsubara I, Horii S, Takeuchi T, Funahashi R, Shikano M, et al. Thermoelectric properties of highly grain-aligned and densified Co-based oxide ceramics. *J Appl Phys* 2003;**93**:2653–8.
28. Lin YH, Lan J, Shen Z, Liu Y, Nan CW, Li JF. High-temperature electrical transport behaviors in textured $Ca_3Co_4O_9$-based polycrystalline ceramics. *Appl Phys Lett* 2009;**94**:072107.
29. Noudem JG, Kenfaui D, Chateigner D, Gomina M. Toward the enhancement of thermoelectric properties of lamellar $Ca_3Co_4O_9$ by edge-free spark plasma texturing. *Scripta Mater* 2012;**66**:258–60.
30. Tani T, Itahara H, Xia C, Sugiyama J. Topotactic synthesis of highly-textured thermoelectric cobaltites. *J Mater Chem* 2003;**13**:1865–7.
31. Itahara H, Sugiyama J, Tani T. Enhancement of electrical conductivity in thermoelectric $[Ca_2CoO_3]_{0.62}[CoO_2]$ ceramics by texture improvement. *Jpn J Appl Phys* 2004;**43**:5134–9.
32. Guilmeau E, Funahashi R, Mikami M, Chong K, Chateigner D. Thermoelectric properties–texture relationship in highly oriented $Ca_3Co_4O_9$ composites. *Appl Phys Lett* 2004;**85**:1490–2.
33. Guilmeau E, Itahara H, Tani T, Chateigner D, Grebille D. Quantitative texture analysis of grain-aligned $[Ca_2CoO_3]_{0.62}[CoO_2]$ ceramics processed by the reactive-templated grain growth method. *J Appl Phys* 2005;**97**:064902.
34. Wang Y, Sui Y, Cheng J, Wang X, Su W, Liu X, et al. Doping-induced metal–insulator transition and the thermal transport properties in $Ca_{3-x}Y_xCo_4O_9$. *J Phys Chem C* 2010;**114**:5174–81.